Computers and Electronics in Agriculture 150 (2018) 152–161

Contents lists available at ScienceDirect

Computers and Electronics in Agriculture

journal homepage: www.elsevier.com/locate/compag

Original papers

Identification and classification of damaged corn kernels with impact acoustics multi-domain patterns

Xuehua Sun[a,b], Min Guo[a,*], Miao Ma[a], Richard W. Mankin[c]

[a] Key Laboratory of Modern Teaching Technology, Ministry of Education, School of Computer Science, Shaanxi Normal University, Xi'an 710062, China
[b] Shaanxi Key Laboratory of Network Data Analysis and Intelligent Processing, School of Computer Science and Technology, Xi'an University of Posts and Telecommunications, Xi'an 710121, China
[c] US Department of Agriculture, Agricultural Research Service, Center for Medical, Agricultural, and Veterinary Entomology, Gainesville, FL 32608, USA

ARTICLE INFO

Keywords:
Impact acoustic signal
Ensemble empirical mode decomposition
Hilbert-Huang Transform
Integration of multi-domain features
Particle swarm optimization-support vector machine

ABSTRACT

An impact acoustic signal device was tested with undamaged, insect-damaged, and mildew-damaged corn kernels, and the different signals were compared using ensemble empirical mode decomposition methods. These methods were adopted based on their known superiority in processing of non-stationary signals and in suppressing of mode mixing. Time domain, frequency domain, and Hilbert domain features were extracted from an ensemble empirical mode decomposition of the impact acoustic signals. Four features were extracted from the time domain: the average amplitude change, Wilson amplitude, average absolute value, and peak-to-peak value. Three features were extracted from the frequency domain: the mean square frequency, the root mean square of the power spectrum, and the frequency band variance. The energy of the high-frequency and low-frequency bands and the average values of the envelopes were extracted from the Hilbert domain. Subsequently, these features were used as inputs to a support vector machine which was optimized by particle swarm optimization. The use of hybrid features enabled higher classification accuracy than usage of features in each domain separately. In this study, achieving the classification accuracies were 99.2% for undamaged kernels, 99.6% for insect-damaged kernels and 99.3% for mildew-damaged kernels. These results, based on ensemble empirical mode decomposition and integration of multi-domain features, are encouraging for the potential of an automated inspection system.

1. Introduction

Insects and mildew often damage grain during storage. These damages reduce grain quality and are a threat to human health. Therefore, prevention of insects and fungal infection has become a serious concern to managers of stored products. Corn is an important stored grain that is easily damaged by insects and mildew. It is necessary to protect the stored corn from any pest and mildew before it is purchased by consumers. With advances in technology, there are more approaches to detect and identify corn kernels, such as machine vision, X-ray imaging and near-infrared (NIR) spectroscopy etc. The X-ray and NIR spectroscopy methods are cost prohibitive and current NIR instrumentation requires complex operating procedures and calibrations (Neethirajan et al., 2007). Moreover, these methods are costly for many commercial applications. Currently, because of its efficiency and convenience, the detection technology using impact acoustics has attracted research attention.

The impact acoustics method was first developed by Pearson and applied to separate pistachio nuts with closed shells from those with open shells. Four features were extracted from each impact acoustic signal in time domain and spectrum analysis (Pearson, 2001). An exhaustive search algorithm was used to select the optimal feature combination, and linear discriminant analysis was used to classify nuts. The identification accuracy of this system was approximately 97%. Later on, analysis of impact acoustic signal characteristics became strong research interest. Onaran et al. (2006) used the same device as Pearson tested to distinguish underdeveloped hazelnuts from fully developed nuts, by calculating and analyzing time domain signal variances and maximum values within short-time windows. In addition, through analysis of the frequency spectra magnitudes and line spectral frequencies, 98.0% of fully developed nuts and 97.0% of underdeveloped hazelnuts were correctly classified. The acoustic signal was processed using four different methods: modeling of the signal in the time-domain, computing time domain signal variances in short time windows, analysis of the frequency spectra magnitudes, and analysis of a derivative spectrum. Features were used as inputs to a neural network.

* Corresponding author.
E-mail address: guomin@snnu.edu.cn (M. Guo).

https://doi.org/10.1016/j.compag.2018.04.008
Received 6 June 2017; Received in revised form 9 April 2018; Accepted 10 April 2018

Pearson et al. (2007) reported that 87% of insect damaged kernels and 98% of the undamaged kernels were correctly classified. Zhongli Pan of United States Department of Agriculture (USDA) developed a system for production of high quality processed beans by applying impact acoustics detection and density separations methods (Pan et al., 2010). Hosainpour et al. (2011) designed an intelligent system used for detection and separation of potatoes from clods. By analyzing the impact acoustic signals in time and frequency domain, 31 different combinations of principle component were selected as input to a back propagation neural network. The network model was determined by evaluation of the mean square error, correct detection rate and correlation coefficient. Detection accuracy of the presented system was about 97.3% and 97.6% for potatoes and clods respectively. Omid (2011) developed a classifier based on expert system for sorting open and closed shell pistachio nuts, which selected the best statistical features with the J48 decision tree (DT). The output of J48 DT algorithm was then converted into crisp IF-THEN rules and membership function sets of the fuzzy classifier. For this model, 99.52% of correct classification on the training set and 95.56% of correct classification on the test set could be achieved. Cetin et al. (2014) designed a system for removing shell pieces from hazelnut kernels. The Mel-cepstral feature parameters, line spectral frequency values, and Fourier-domain Lebesgue features were extracted from the impact acoustic signals. The feature parameters were classified using a support vector machine (SVM), whereby an average recognition rate of 98.2% was achieved. However, it was not studied in-depth how to effectively interpret the impact acoustic signal.

It should be pointed out that through previous literatures had made many efforts in obtaining satisfactory accuracy. Summarized the previous research methods of signal processing, found that features extracted by the traditional methods were relatively single. Thus it cannot fully reflect the essential characteristics of the signal, result in lower separability of signals. Almost no literature extracted features by applying multi-domain method which can be used to obtain additional information and maximum separability. This motivated us to exploit the integration of multi-domain to analyse the impact acoustic signals. Features which were extracted from the original impact acoustic signals mainly reflect the general characteristics of signals rather than the local characteristics. Ensemble empirical mode decomposition (EEMD), which was based on the local characteristic time scale of a signal, can self-adaptively process non-stationary signals and suppress mode mixing. After using EEMD for the impact acoustic signals, it can decompose the signals into different frequency bands and will be helpful for further analysing the signals. In addition, the detection system was easy to acquire and low-cost. Therefore, the system was suitable for which the high precision was indeed required (Weaver et al., 1997).

This paper had the following main contributions. First, based on its capability to process non-stationary signals and its suppression of mode mixing, EEMD algorithm was used in this paper. Second, in order to extract the essential features of impact acoustic signals and has a higher separability of signals, integration of multi-domain method was proposed to deal with the impact acoustic signals. Third, to find the optimal parameters so as to overcome the flaws of conventional methods of SVM, the particle swarm optimization-support vector machine (PSO-SVM) was used.

2. Experimental apparatus and materials

2.1. Hardware

The experimental apparatus included a vibration feeder, a microphone, an impact plate and a computer equipped with a sound card (Fig. 1). Its main functions are: (1) the vibration feeder conveys the corn kernels from the bulk hopper into a single-flow by the time they reached the end of the feeder; (2) the Shure BG4.1 cardioid condenser microphone detects the impact signals using a pickup with a broadband frequency response. The frequency response of Shure BG4.1 is from 40 Hz to 18 kHz; and (3) the impact plate provides a high-mass impact point that maximizes the amplitude of grain vibrations and minimizes vibration from the plate itself. Through trial and error, the impact plate is optimized to be a block of stainless steel approximately 24 cm × 12 cm × 0.05 cm. The drop distance from the feeder to the impact plate is set at 40 cm and the plate is inclined at 60° above the horizontal. A MAYA44 sound card equipped with 4 output channels and 4 input channels is used to interface to the signal processing computer. The frequency range of the sound card is 20 Hz–20 KHz, and the microphone signals are digitized at a sampling frequency of 48 KHz with 16bit resolution.

2.2. Experiment material

Three types of corn samples were from the same batches, including undamaged kernels (UDK), insect-damaged kernels (IDK) and mildew-damaged kernels (MDK), as shown in Fig. 2. The corn kernels (UDK, IDK, MDK) were 280 each and 840 in total. The corn samples dropped onto the impact plate, and then the acoustic signals were collected by the microphone. The impact acoustic signals were acquired and stored in WAV format, which were used later for processing.

3. Method

3.1. Signal processing method

3.1.1. Ensemble empirical mode decomposition

The empirical mode decomposition (EMD) method (Huang et al., 1998) was compared with traditional time-frequency analysis methods, such as short-time Fourier transform, wavelet analysis. EMD is based on the local characteristics time scale of the signal and can adaptively decompose a complicated signal into a sum of intrinsic mode functions (IMF). EMD method has been applied widely to signal processing (Li et al., 2014; Li et al., 2015). However, a major drawback to general usage of EMD is mode mixing, in which signals of similar scale reside in different IMF components or a single IMF consists of signals of disparate scale (Huang and Wu, 2008). To alleviate the mode mixing in EMD, EEMD was presented by Wu and Huang (2009). EEMD is a noise-assisted data analysis method, which adds finite white noise to the investigated signal and then decomposes the complicated signal into a set of complete and almost orthogonal components. Because this method suppresses mode mixing effectively, the EEMD has been applied widely for signal detection and fault diagnosis (e.g., Amirat et al., 2013; Wang et al., 2014).

The EEMD algorithm can be given as follows:

(1) Add a white noise series to the investigated signal,

$$X_m(t) = x(t) + n_m(t), \quad m = 1, 2, \cdots, M \tag{1}$$

where $x(t)$ represents the investigated signal, $n_m(t)$ indicates the mth added white noise series, and $X_m(t)$ represents the noise-added signal of the mth trial.

(2) Decompose the noise-added signal $X_m(t)$ into IMF component $c_{i,m}$, using the EMD method. where $c_{i,m}$ represents the i th IMF component of the mth trial.
(3) Add different white noise series to the investigated signal, repeat step (1) and step (2) again for M trials.
(4) Calculate the ensemble mean $\bar{c}_i(t)$ of the M trials for each IMF.

$$\bar{c}_i(t) = \frac{1}{M}\sum_{m=1}^{M} c_{i,m}(t),\ i = 1, 2, \cdots I, \quad m = 1, 2, \cdots, M \tag{2}$$

where I is the number of IMF components.

(5) Eventually, the investigated signal can be represented as follows:

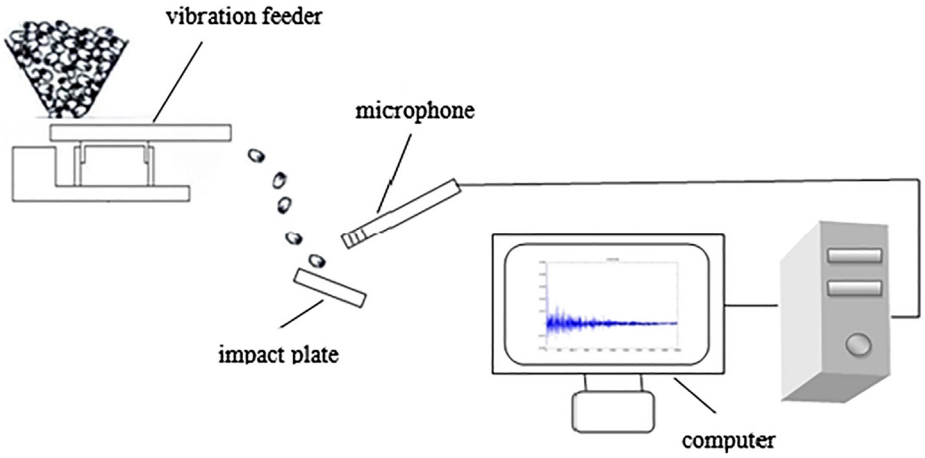

Fig. 1. Experimental apparatus.

Fig. 2. Three types of corns (a) UDK; (b) IDK; (c) MDK.

$$x(t) = \sum_{i=1}^{I} c_i(t) + r_I(t) \tag{3}$$

where $c_i(t)$ represents the ith IMF component, and $r_I(t)$ is the residue.

3.1.2. Parameter setting in EEMD

The number of ensemble trials, M, and the noise amplitude were two parameters that need to be set empirically when the EEMD method was used. To demonstrate how to select the two parameters, Wu and Huang used different amplitude ratios namely 0.1, 0.2 and 0.4 of standard deviations of investigated signals. From the result, it is suggested the amplitude of added white noise is approximately 0.2 standard deviations of the investigated signal, and the ensemble number of the above case is 100 (Wu and Huang 2009). In this study, the amplitude ratio was 0.2 and the number of ensemble trials was 100.

As the maximum amplitude of impact acoustic signal was well above background levels, it was easy to separate each of impact acoustic signals. We used a thresholding method based on the maximum amplitude of impact acoustic signal. We acquired 2048 data points which began 48 points in front of the maximum magnitude of the whole signal. Typical signals from an UDK, an IDK and a MDK are shown in Fig. 3. The maximum amplitude of the signals is quite variable but the overall shape of signals from the three types of kernel is more consistent. As demonstrated in time domain, the difference among three types of signals amplitude fluctuations is very large and time domain waveform changes is different, so we can extract the features from these signals.

The three kinds of impact acoustic signals are shown in Fig. 4 in the frequency domain. The overall trend of the three kinds varied with frequency, as well the maximum amplitude. Different frequency components emerged in the three types of signals, which enabled different signal features to be extracted from different frequency bands.

The impact acoustic signal of an UDK is used as an example for EEMD decomposition of a signal (Fig. 5). It is clear that the information in the signal is obtained primarily from the first several IMF components and the most important signal features could be extracted from these first several components.

3.1.3. Hilbert transform

The Hilbert transform of $c_j(t)$ can be performed using the formula:

$$H[c_j(t)] = p.\ \frac{1}{\pi}\int_{-\infty}^{\infty} \frac{c_j(\tau)}{t-\pi} dt \tag{4}$$

where P denotes Cauchy principal component. The analytic signal can be generated as:

$$A[c_j(t)] = c_j(t) + iH[c_j(t)] = a_j(t)e^{i\theta_j(t)} \tag{5}$$

where,

$$a_j(t) = \sqrt{c^2{}_j(t) + H^2[c_j(t)]} \tag{6}$$

$$\theta_j(t) = \arctan \frac{H[c_j(t)]}{c_j(t)} \tag{7}$$

where $a_j(t)$ and $\theta_j(t)$ are the instantaneous amplitude and instantaneous phase respectively. The time derivative of the instantaneous phase $\theta_j(t)$ is the instantaneous frequency $\omega_j(t)$. The frequency can be obtained as:

$$\omega_j(t) = \frac{d\theta_j(t)}{dt} \tag{8}$$

From Eq. (4) to Eq. (8), the Hilbert transform of each IMF

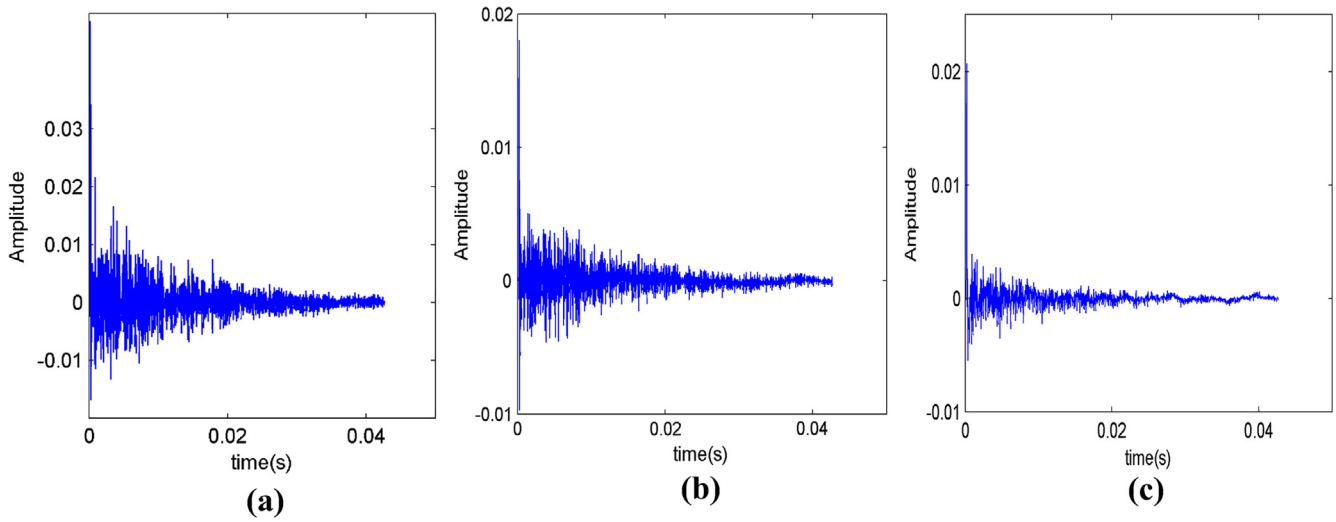

Fig. 3. Examples of impact acoustic signals in time domain (a) UDK; (b) IDK; (c) MDK.

component can be performed as follow:

$$c_j(t) = \mathrm{Re}\left[a_j(t)e^{i\theta_j(t)}\right] = \mathrm{Re}[a_j(t)e^{i\int \omega_j(t)dt}] \tag{9}$$

The Hilbert spectrum analysis of $x(t)$ can be defined as:

$$x(t) = \mathrm{Re}[a_j(t)e^{i\int \omega_j(t)dt}] + r_n \tag{10}$$

where r_n denotes the residual component, which reflects the average trend of $x(t)$. The features should be extracted from the first several IMF components, so the residual component is not considered.

3.1.4. Time domain features

As was demonstrated in the time domain, the amplitude fluctuations of the three types of signals were relatively large. Four features, namely the average amplitude change (AAC), Wilson amplitude (WAMP), average absolute value (AAV) and peak-to-peak value (PK-PK), were extracted from the time domain. Mathematical equations and the specific signal meaning of every feature in time domain are: N is the number of sample points and $c_{i,k}$ represents the amplitude of the ith IMF component of the kth trial. The AAC showed a significant change in the average amplitude of the impact acoustic signals:

$$AAC = \frac{1}{N}\sum_{i=1}^{N} |c_{i+1,k} - c_{i,k}| \tag{11}$$

The WAMP is the number of times that the difference between impact acoustic signal amplitude among two adjacent time segments exceeds a predefined threshold. This feature can record the change of the amplitude of the impact acoustic signal, when the change exceeds a threshold value, this value plus 1. The WAMP be expressed as follows:

$$WAMP = \sum_{i=1}^{N} f(|c_{i,k} - c_{i-1,k}|);$$

$$f(x) = \begin{cases} 1 & if\ x \geqslant threshold \\ 0 & x < threshold \end{cases}. \tag{12}$$

AAV reflect the central tendency of signal change and can be defined as:

$$AAV = \frac{1}{N}\sum_{i=1}^{N} c_{i,k} \tag{13}$$

PK-PK is the differences between the highest and lowest in a cycle, that is to say, the range between the maximum and the minimum. It describes the range of signal variation and can be calculated by:

$$PK\_PK = \max(c_{i,k}) - \min(c_{i,k}) \tag{14}$$

Visual representations are presented in Fig. 6, where the red marks, blue marks, and green marks represent the feature values of UDK, IDK, and MDK, respectively. Those features are extracted from IMF1 and indicate that the damaged kernels (IDK, MDK) can be distinguished from UDK by using the time domain features.

3.1.5. Frequency domain features

Three features were obtained from the frequency domain named mean square frequency (MSF), root mean square of power spectrum (RMSPS) and frequency band variance (FBV).

The Fast Fourier Transform (FFT) is applied on the original signal and then extracts the mean value of the amplitude. That is to say, the MSF describes the change of the center position of the spectrum and can

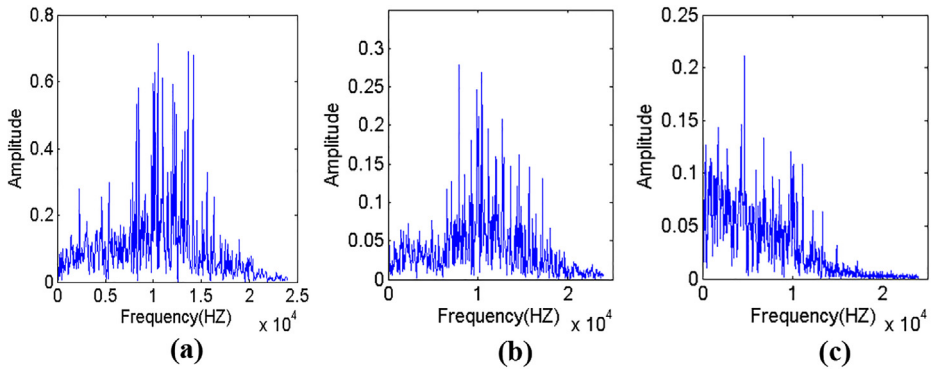

Fig. 4. Impact acoustic signals in frequency domain (a) UDK; (b) IDK; (c) MDK.

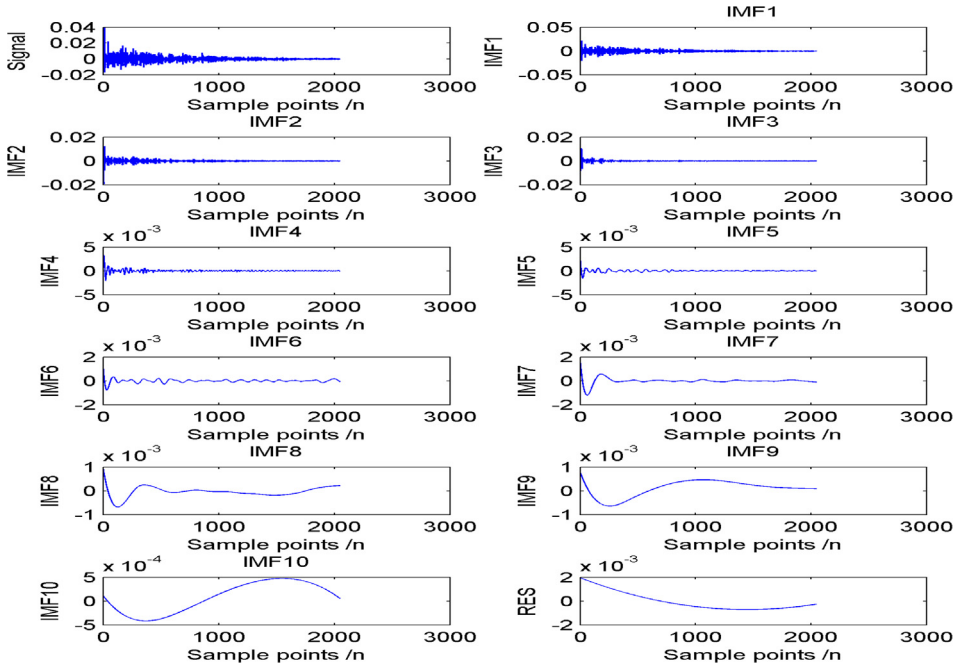

Fig. 5. The EEMD decomposition from an impact acoustic signal of UDK.

be defined as:

$$MSF = \frac{1}{M}\sum_{k=0}^{M-1} X(k) \tag{15}$$

where M is the number of sample points, and $X(k)$ represents the amplitude of the Fourier transform.

The direct method of power spectrum is used in this paper. The RMSPS is used as a feature and reflects the dispersion degree of spectral energy distribution of power. It can be calculated by:

$$RMSPS = \sqrt{\frac{1}{M}\sum_{i=1}^{M} X_i^2} \tag{16}$$

where M is the number of sample points, and X_i represents the amplitude of the power spectrum.

The FBV indicates the energy variance of the signal in different frequency bands, and the physical meaning is that the fluctuation characteristic and short time energy characteristic of each frequency band:

$$FBV = \frac{1}{M}\sum_{k_1=0}^{M-1}\left[X(k_1) - \frac{1}{M}\sum_{k=0}^{M-1} X(k)\right]^2 \tag{17}$$

where M is the number of sample points, and $X(k)$ represents the amplitude of the Fourier transform.

As see from Fig. 7, the red curve, the blue curve, the green curve represent the frequency domain feature values of UDK, IDK and MDK, respectively. The signal fluctuations have been differently pronounced in three regions. Although there is little confusion among the three curves, it can indicate that the damaged corn kernels (IDK, MDK) can be identified by these features.

3.1.6. Hilbert domain features

The energy of the 10–15-kHz high frequency band (ENH), the energy of the 5–10-kHz low frequency band (ENL), and the average value of envelope (AVE) were extracted from the Hilbert domain.

(1) ENH and ENL

The IMFs were acquired by EEMD for the original signal, and the Hilbert spectrum was obtained by the Hilbert-Huang Transform (HHT) for each IMF. The 5–15 kHz frequency range was divided into two parts; 5–10 kHz included the low frequency band, and 10–15 kHz, the high frequency band. According to the Parseval theorem, the total energy of signal $x(t)$:

$$E = \sum_{k=1}^{N} x_k^2 \tag{18}$$

where, x_k indicates the amplitude of signal at the k sampling point.

There are N sampling points for the ith IMF, where the instantaneous frequency of j sampling points is $f_{i,j}$, and the instantaneous amplitude is $a_{i,j}$. The instantaneous intensity is $A_{i,j} = a_{i,j}^2 (i = 1, 2, \cdots, n)$. The instantaneous intensity of the sampling points in the high frequency band and the low frequency band is $A_{h,j}$ and $A_{l,j}$ respectively. The total energy of the high frequency band and the low frequency band is *ENH* and *ENL* respectively:

$$ENH = 10\ln\sum_{j=1}^{N} A_{h,j} \tag{19}$$

$$ENL = 10\ln\sum_{j=1}^{N} A_{l,j} \tag{20}$$

(2) AVE

The envelope curves can be obtained by applying Hilbert transform for each of IMF. The AVE reflects size of envelope fluctuation and uses the following formula:

$$AVE = \frac{1}{M}\sum_{i=1}^{M} envelope(i) \tag{21}$$

As see from Fig. 8, these characteristics indicate that damaged kernels (IDK, MDK) can be distinguished successfully from undamaged kernels by using the selected features.

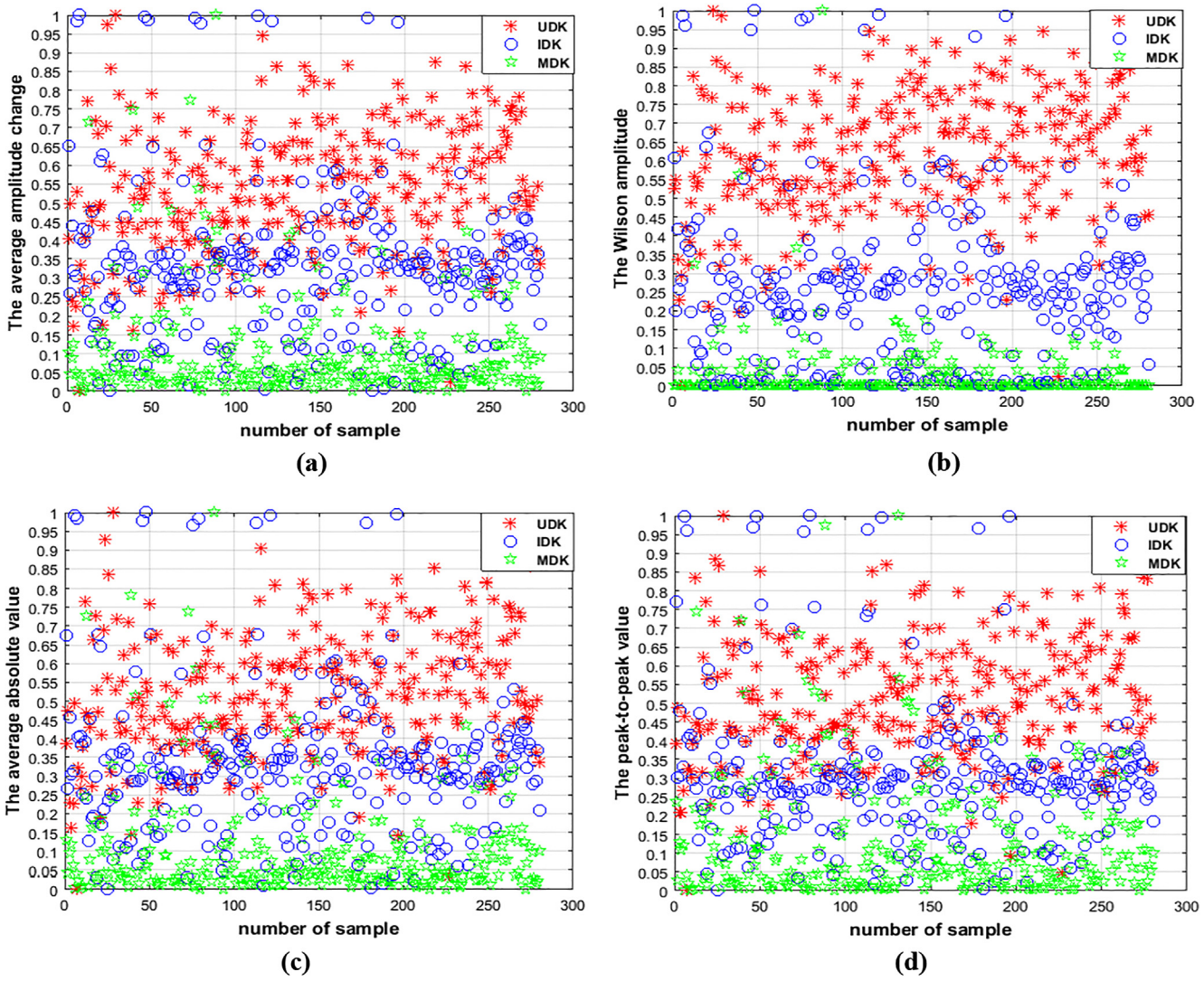

Fig. 6. Scatter diagram of time domain features (a) AAC; (b) WAMP; (c) AAV; (d) PK-PK.

3.2. Classification method

3.2.1. Support vector machine classifier

SVM classifier is a supervised learning algorithm based on statistical learning theory. SVM is a prediction tool with good generalization ability. It effectively solves the real problems of the small sample, nonlinear, high-dimension, the local minimum value, and so on, has a good classification results. In SVM, the original input space is mapped into a high-dimensional dot product space called a feature space, and in the feature space, the optimal hyperplane is determined to maximize the generalization ability of the classifier. Let n-dimensional input $x_i (i = 1 \cdots M)$, (M be the number of samples), associated labels be $y_i = 1$ for Class I and $y_i = -1$ for Class II. For linearly separable data, we can determine a hyperplane $f(x) = 0$ that separates the data.

$$f(x) = \omega^T x + b = \sum_{j=1}^{n} \omega_j x_j + b = 0 \tag{22}$$

where ω is an n-dimensional vector and b is a scalar. The vector ω and the scalar b determine the position of the separating hyperplane. Function Sign is also called the decision function. A separating hyperplane satisfies the constraints $f(x_i) \geqslant 1$ if $y_i = 1$ for Class I and $f(x_i) \geqslant -1$ if $y_i = -1$ for Class II. This results in (23).

$$y_i f(x_i) = y_i(\omega^T x_i + b) \geqslant 1 \quad i = 1, \cdots, M \tag{23}$$

The separating hyperplane that creates the maximum distance between the plane the nearest data (i.e., the maximum margin) is called the optimal separating hyperplane. Taking into account the noise with slack variables ξ_i and error penalty c, the optimal hyperplane can be found by solving the following convex quadratic optimization problem:

minimize

$$\frac{1}{2} \|\omega\|^2 + c \sum_{i=1}^{M} \xi_i \tag{24}$$

subject to

$$y_i(\omega^T x_i + b) \geqslant 1 - \xi_i, \quad i = 1, \cdots, M, \ \xi_i \geqslant 0 \tag{25}$$

where ξ_i is measuring the distance between the margin and the examples $x_i$lying on the wrong side of the margin. SVM models the pattern recognition problem as a convex quadratic programming in feature space, which can be transformed into the following optimal problem by constructing the Lagrange function:

$$\min \frac{1}{2} \sum_{i=1}^{j} \sum_{j=1}^{l} y_i y_j \alpha_i \alpha_j K(y_i, y_j) - \sum_{j=1}^{l} \alpha_j \tag{26}$$

$$s.t. \sum_{i=1}^{l} y_i \alpha_i = 0, \ 0 \leqslant \alpha_i \leqslant c, \quad i = 1, \cdots, l \tag{27}$$

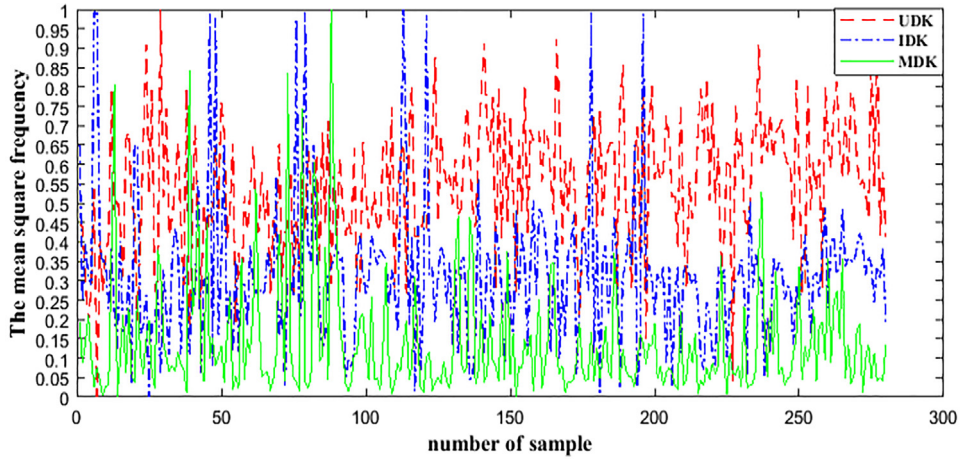

(a)

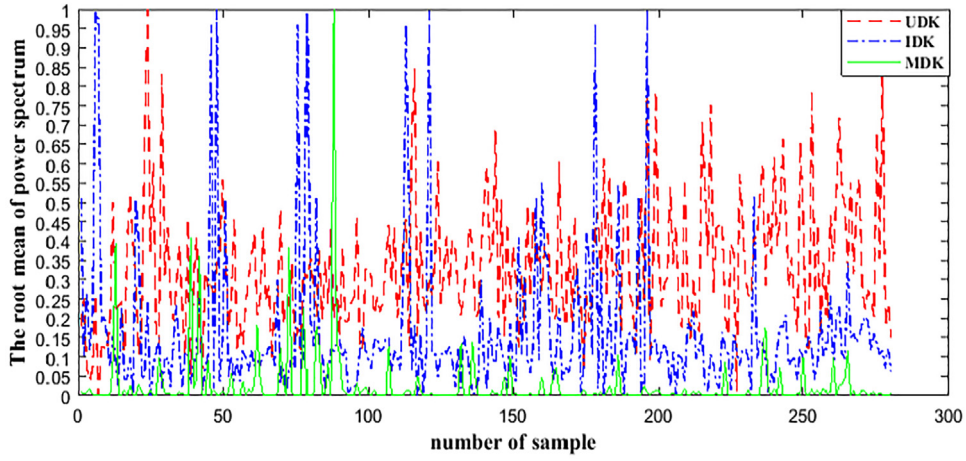

(b)

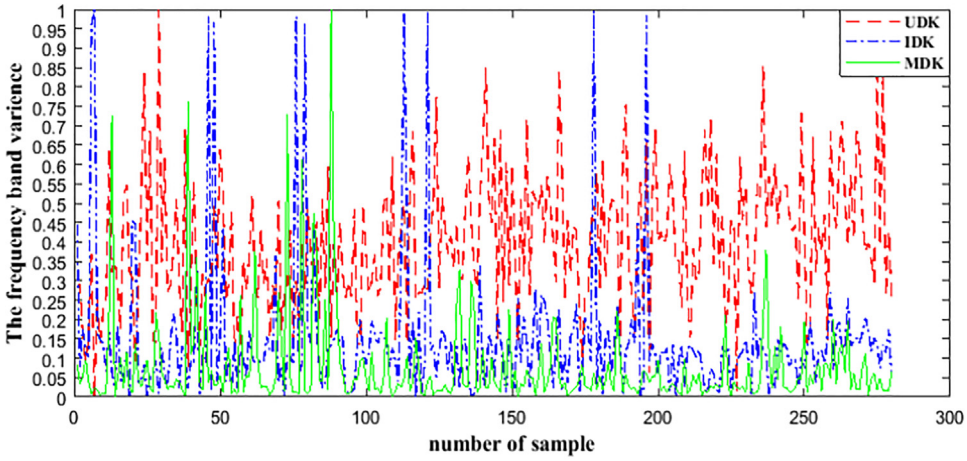

(c)

Fig. 7. Frequency domain features from three types of impact acoustic signals (a) MSF; (b) RMSPS; (c) FBV.

where $\alpha = [\alpha_1, \alpha_2, \cdots, \alpha_N]$ is the vector of the Lagrange.

In the optimization problem, we need first to determine the kernel function, $K(X_i, X_j)$. A radial basis function (RBF) is used in the study and defined as:

$$K(X_i, X_j) = \exp(-g \|x_i - x_j\|^2), g > 0 \quad (28)$$

A particle swarm optimization algorithm, PSO, was used to select the penalty parameter c and kernel function parameter g to improve the classification effect of SVM.

3.2.2. Particle swarm optimization algorithm

The PSO algorithm was proposed by Eberhart and Kennedy. PSO was presented under the inspiration of bird flock immigration during the course of finding food. The PSO employs a swarm of particles that

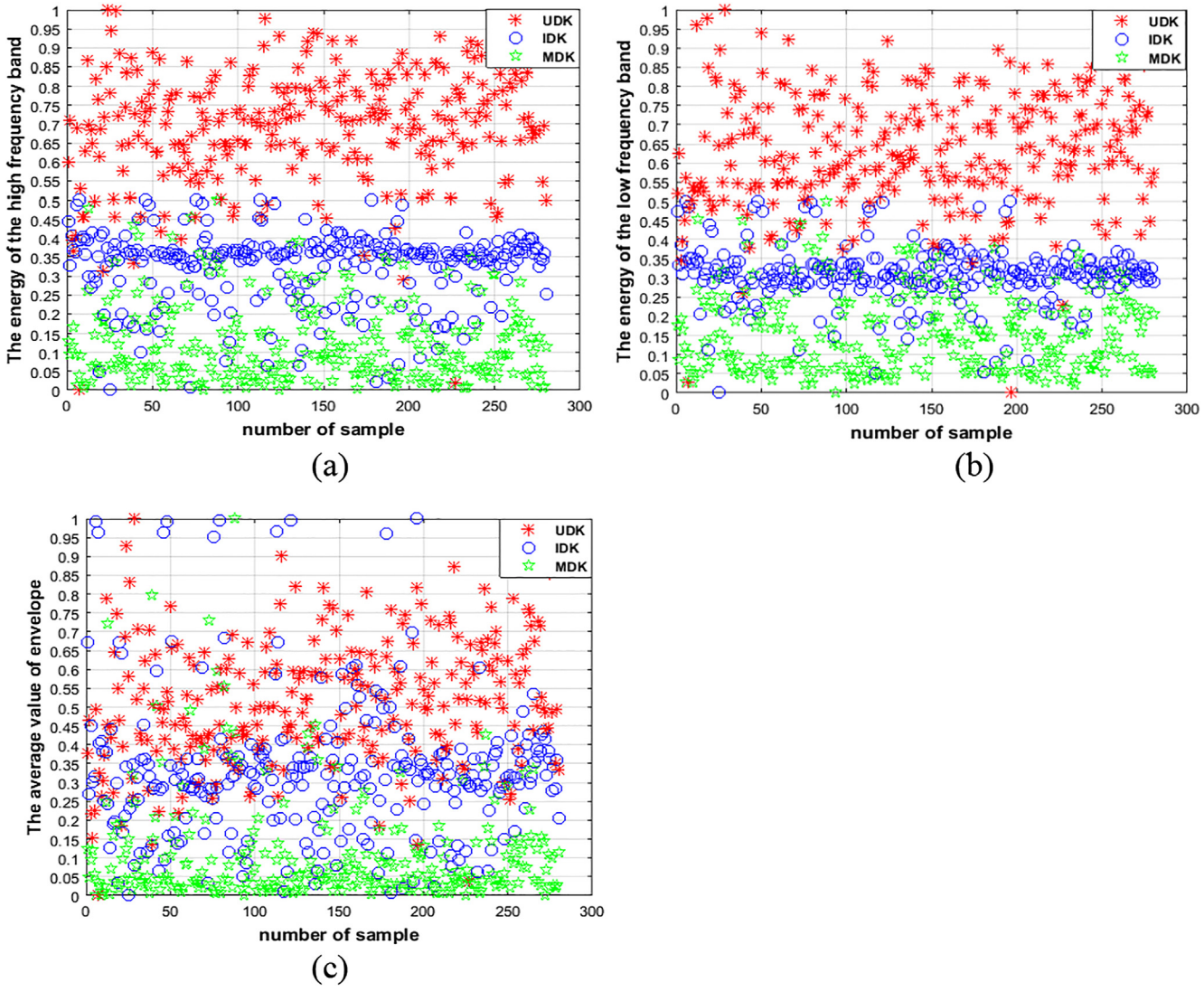

Fig. 8. Hilbert domain features from three types of impact acoustic signals (a) ENH; (b) ENL; (c) AVE.

search for the best position with respect to the corresponding best solution for an optimization problem in the virtual search space. It is widely used in solving the optimization problems (Jiang et al., 2007). The PSO algorithm works by having a population (called a swarm) of candidate solutions (called particles). These particles are moved around in the search space according to a few simple formulae. The movements of the particles are guided by their own best known position in the search space as well as the entire swarm's best known position. The process is repeated until that a satisfactory solution is discovered. Formally, let f: $R^n \rightarrow R$ be the function which needs to be minimized. The gradient of f is not known. The goal is to find a solution A for which $f(A) \leqslant f(B)$ for all in the search space. That is to say, the solution A is the global minimum. Maximization can be performed by considering the function $h = -f$ instead. In PSO, each solution is regarded as a particle in search space. Each particle has a fitness value which determined by a target function. The status of each particle includes its position and velocity. $X_i = (x_{i1}, x_{i2}, \cdots, x_{ie})$ is the position of the ith particle in the n-dimensional search space, and $V_i = (v_{i1}, v_{i2}, \cdots, v_{ie})$ is the velocity of the ith particle, where $i = 1, 2, \cdots, n$, n is the number of species, and e is the dimension of the search space. At each time k, the PSO algorithm updates the velocities and positions of the particle, respectively, using the equations:

$$v_{ie}^{k+1} = \omega * v_{ie}^{k} + c_1 * rand_1^k() * (p_{ie}^k - x_{ie}^k) + c_2 * rand_2^k() * (p_{ge}^k - x_{ie}^k) \quad (29)$$

$$x_{ie}^{k+1} = x_{ie}^{k} + v_{ie}^{k+1} \quad (30)$$

where ω is called the inertial weight coefficient. It is a proportion factor concerned with former velocity. c_1 and c_2 are learning factors, and $rand_1$ and $rand_2$ are positive random number between 0 and 1 under normal distribution. $p_i = (p_{i1}, p_{i2}, \cdots, p_{ie})^T$ is the personal best position of particle i, $p_g = (p_{g1}, p_{g2}, \cdots, p_{ge})^T$ denotes the best one of all personal best positions of all particles within the swarms. This updating produce continues until it reaches the maximum number of iterations, which is set at the beginning.

3.2.3. Particle swarm optimization-support vector machine classifier

In this study, PSO is used to select the penalty parameter c, and kernel function parameter g. The most important advantages of the PSO are that PSO is easy to implement and there are few parameters to adjust (Nickabadi et al., 2011). Escalante et al. (2009) provide empirical evidence indicating that by using PSO it is able to perform intensive search over a huge space and succeeded in selecting competitive models without significantly overfitting. This is due to the way the search is guided in PSO: performing a broad search around promising solutions but not overdoing in terms of really fine optimization. We describe the process of parameters optimization of SVM with PSO as: (1) Initialize all particles' positions and velocity; (2) Train a SVM classifier using the acoustic signals, and then use the cross validation

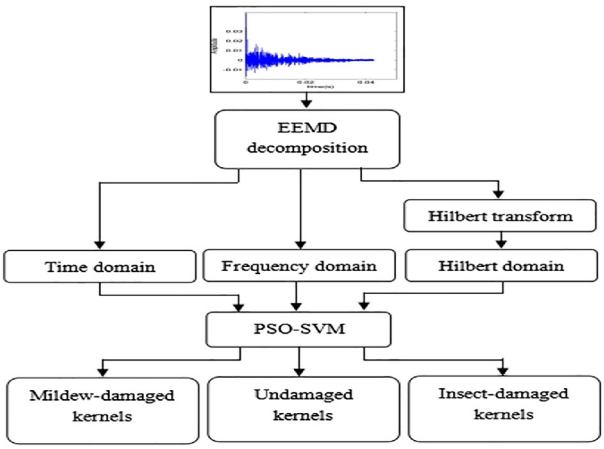

Fig. 9. The frame diagram of the sorting model.

method to calculate every particle's fitness; (3) update the individual extremum and global value according to the fitness; (4) update the velocity and position for every particle using Eqs. (29) and (30); (5) Stop if the number of iterations is satisfied; otherwise go back to step (2).

The frame diagram of the sorting model is shown in Fig. 9. Matlab data acquisition toolbox was used for preserving the impact acoustic signals of UDK, IDK and MDK. The IMFs were acquired by EEMD decomposition. Features were extracted from the time domain, the frequency domain and the Hilbert domain respectively. Subsequently, these features were input to PSO-SVM.

840 corn kernels, including 280 UDK, 280 IDK and 280 MDK, were used in the experiment. We used 10-fold cross-validation, dividing the set of samples at random into 10 approximately equal-size parts. The 10 parts were roughly balanced, ensuring that the classes were distributed proportionally among each of the 10 parts. 10-fold cross-validation works as follows: We fit the PSO-SVM on 90% of the samples and then predict the class labels of the remaining 10% (the test samples). This procedure was repeated 10 times, then the average accuracies across all 10 trials was computed.

4. Results

4.1. Time domain features

Correct detection rates for different combinations of features in the time domain are shown in Table 1. The recognition rate of MDK is the lowest compared with UDK and IDK. The recognition rate of MDK increases considerably when making use of combined features, and the optimal feature combination of all features resulted in classification accuracies of 98.7%, 96.5%, 95.4% for UDK, IDK and MDK respectively.

Table 1
Classification accuracies for subsets of time domain features.

Time domain features	Number of features	Correct detection rate (%)		
		Undamaged kernels	IDK	MDK
I AAC	2	96.1	98.5	85.8
II WAMP	2	93.6	97.6	85.2
III AAV	2	97.8	96.5	85.9
IV MAX-MIN	2	98.2	91.2	87.2
I + II	2 + 2	97.2	98.2	88.3
I + III	2 + 2	98.3	98.9	90.0
I + IV	2 + 2	98.1	98.7	90.4
II + III	2 + 2	96.8	98.5	89.6
II + IV	2 + 2	92.9	99.2	91.2
III + IV	2 + 2	98.9	98.9	88.2
I + II + III	2 + 2 + 2	98.5	99.4	93.4
I + II + IV	2 + 2 + 2	97.2	96.5	91.2
I + III + IV	2 + 2 + 2	98.1	97.6	91.5
II + II + IV	2 + 2 + 2	98.7	94.9	91.3
I + II + III + IV	2 + 2 + 2 + 2	**98.7**	**96.5**	**95.4**

Table 2
Classification accuracies for subsets of frequency domain features.

Frequency domain features	Number of features	Correct detection rate (%)		
		Undamaged kernels	IDK	MDK
I MSF	2	94.2	97.9	84.1
II RMSPS	2	97.6	96.8	85.7
III FBV	2	95.7	85.4	97.1
I + II	2 + 2	93.9	95.3	94.9
I + III	2 + 2	97.9	96.1	91.9
II + III	2 + 2	96.1	90.3	97.6
I + II + III	2 + 2 + 2	**98.2**	**97.9**	**97.5**

4.2. Frequency domain features

Correct detection rates for different combinations of frequency domain features, MSF, RMSPS, and FBV, are listed in Table 2. The classification accuracy rate is increased when making used of combined features. Using the PSO-SVM classifier, the highest classification accuracies are achieved as 98.2%, 97.9%, 97.5% for UDK, IDK and MDK respectively.

4.3. Hilbert domain features

The change trends of the average value of IMF envelope for the three types of corn kernel are described in Fig. 10. The curves for all three types of corn kernel present a general downward trend. It is evident that the average IMF envelope is largest for undamaged kernels among the three types of corn kernels only for the first 3 IMF components. Therefore, the feature is extracted from IMF1, IMF2 and IMF3 in this study.

As with the time domain and frequency domain features, the detection rates for the three types of kernel are relatively lower when using only a single Hilbert domain feature and the classification accuracy rate of MDK increases when making use of combined features. Using optimized PSO-SVM classifier, correct detection rates are 99.1%, 96.3%, 95.1% for UDK, IDK and MDK, respectively (Table 3).

4.4. Hybrid domain features

Different combinations of the classification features are show in Table 4 for identification of subsets of optimal features. With the combination of different domain features, the overall recognition rate is improved further. Ultimately, the Hybrid domain features can be achieved optimal classification results. The recognition rate of PSO-SVM classifier is higher than that of SVM classifier.

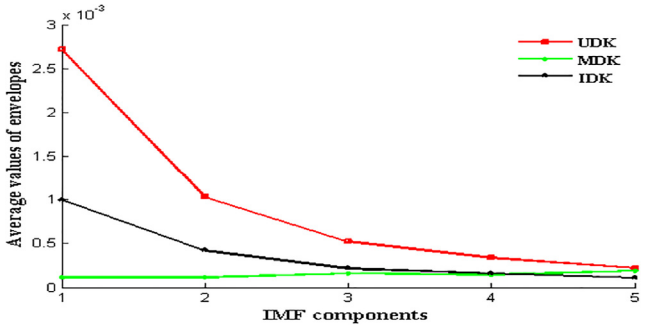

Fig. 10. Average value of IMF envelope.

Table 3
Classification accuracies for subsets of Hilbert domain features.

Hilbert domain features	Number of features	Correct detection rate (%)		
		Undamaged kernels	IDK	MDK
I ENH	1	96.2	94.4	86.1
II ENL	1	97.9	98.2	85.2
III AVE	3	98.2	92.6	87.2
I + II	1 + 1	96.9	94.2	91.2
I + III	1 + 3	91.5	98.2	89.1
II + III	1 + 3	97.5	98.5	89.6
I + II + III	1 + 1 + 3	**99.1**	**96.3**	**95.1**

Table 4
Classification accuracies for subsets of Hybrid domain features.

Features	Number of features		Correct detection rate (%)	
			SVM	PSO-SVM
I time domain	8	UDK	97.8	98.9
		IDK	95.8	96.2
		MDK	78.2	95.3
II frequency domain	6	UDK	94.7	96.9
		IDK	93.7	97.9
		MDK	92.2	96.8
III Hilbert domain	5	UDK	93.1	97.6
		IDK	94.7	96.9
		MDK	84.8	96.8
I + II + III	19	UDK	98.1	**99.2**
		IDK	91.7	**99.6**
		MDK	92.6	**99.3**

5. Discussion

Although the time and frequency domain features of the acoustic impact signals collected in this study can be extracted directly from the original signals, it was necessary to optimize their application using the self-adaptation properties of EEMD analysis. The features extracted from the original signals mainly reflect the overall signal, ignoring its evolution over time. The EEMD method self-adapted according to the local time-varying characteristic to decompose the complicated signal into a set of IMF components that revealed more differences among the signals than could be observed directly from the original signals. Feature extraction through the EEMD method can reveal the different IMFs over which the features are separable for different corn kernel types and thus are useful for improved classification accuracy.

The signal classification information was contained primarily in the first several IMFs. Further analysis indicated that the features extracted from IMF1 and IMF2 provided the greatest precision for revealing the different characteristics of the signals. Consequently, the time domain features and the frequency domain features were extracted from IMF1, IMF2 in this study. ENH, ENL, AVE were extracted from Hilbert domain. The ENH and ENL were extracted from IMF1, because IMF1 highlights the main frequency components of EEMD decomposition. Therefore, the Hilbert spectrum was obtained by HHT from IMF1, and then ENH and ENL were extracted from it. From Fig. 9, we can see the AVE should be extracted from IMF1, IMF2, and IMF3.

6. Conclusions

The experimental results suggest the following conclusions: (1) The differences among the detection accuracies for the three types of corn kernels is large when using a single feature. (2) Combined features have better classification accuracy rates than a signal feature derived from the time domain, frequency domain and Hilbert domain. (3) The integration of information from multiple transform domains can provide additional accuracy and maximum class separability. (4) The identification accuracy rate is higher using the PSO-SVM than the SVM.

The results obtained from this study prove that the EEMD and integration of multi-domain can increase the separability of extracted features efficiently and contribute to identify of damaged corn kernels (IDK, MDK). The EEMD method provides a new way for detecting corn quality and decreasing storage losses. The method has potential for use also with wheat, beans and other stored grains.

Acknowledgements

This work was supported by the National Natural Science Foundation of China (Grant No. 11372167), the Science Research and Development Program of Shaanxi Province of China (No. 2016NY-176), Interdisciplinary Incubation Project of Learning Science of Shaanxi Normal University.

References

Amirat, Y., Choqueuse, V., Benbouzid, M., 2013. EEMD-based wind turbine bearing failure detection using the generator stator current homopolar component. Mech. Syst. Signal Process. 41 (1–2), 667–678.
Cetin, A.E., Pearson, T.C., Sevimli, R.A., 2014. System for removing shell pieces from hazelnut kernels using impact vibration analysis. Comput. Electron. Agric. 101, 11–16.
Escalante, H.J., Montes, M., Sucar, L.E., 2009. Particle swarm model selection. J. Mach. Learn. Res. 10 (2), 405–440.
Jiang, Y., Hu, T., Huang, C., Wu, X., 2007. An improved particle swarm optimization algorithm. Appl. Math. Comput. 193 (1), 231–239.
Hosainpour, A., Komarizade, M.H., Mahmoudi, A., Shayesteh, M.G., 2011. High speed detection of potato and clod using an acoustic based intelligent system. Exp. Syst. Appl. 38 (10), 1–6.
Huang, N.E., Shen, Z., Long, S.R., Wu, M.C., Shi, H.H., Zheng, Q.N., Yen, N.C., Tang, C.C., Liu, H.H., 1998. The empirical mode decomposition and the Hilbert spectrum for nonlinear and non-stationary time series analysis. Proc. Roy. Soc. London 454, 903–995.
Huang, N.E., Wu, Z., 2008. A review on Hilbert-Huang transform: method and its applications to geophysical studies. Rev. Geophys. 46 (2), RG2006.
Li, H.Q., Wang, X.F., Chen, L., Li, E.B., 2014. Denoising and R-peak detection of electrocardiogram signal based on EMD and improved approximate envelope. Circ., Syst., Signal Process 33 (4), 1261–1276.
Li, M., Wu, X., Liu, X.Y., 2015. An improved EMD method for Time-frequency feature extraction of telemetry vibration signal based on multi-scale median filtering. Circ., Syst., Signal Process 34 (3), 815–830.
Neethirajan, S., Karunakaran, C., Jayas, D.S., White, N.D.G., 2007. Detection techniques for stored-product insects in grain. Food Control 18 (2), 157–162.
Nickabadi, A., Ebadzadeh, M.M., Safabakhsh, R., 2011. A novel particle swarm optimization algorithm with adaptive inertia weight. Appl. Soft Comput. 11 (4), 3658–3670.
Pearson, T.C., 2001. Detection of pistachio nuts with closed shells using impact acoustics. Appl. Eng. Agric. 17 (2), 249–253.
Onaran, I., Pearson, T.C., Yardimci, Y., Cetin, A.E., 2006. Detection of underdeveloped hazelnuts from fully developed nuts by impact acoustics. Trans. ASABE 49 (6), 1971–1976.
Omid, M., 2011. Design of an expert system for sorting pistachio nuts through decision tree and fuzzy logic classifier. Exp. Syst. Appl. 38 (4), 4339–4347.
Pearson, T.C., Cetin, A.E., Tewfik, A.H., Haff, R.P., 2007. Feasibility of impact-acoustic emissions for detection of damaged wheat kernels. Digital Signal Process. 17 (13), 617–633.
Pan, Z.L., Atungulu, G.G., Wei, L., Haff, R., 2010. Development of impact acoustic detection and density separations methods for production of high quality processed beans. J. Food Eng. 97 (3), 209–300.
Weaver, D.K., Shuman, D., Mankin, R.W., 1997. Optimizing and assessing the performance of an algorithm that cross-correlates acquired acoustic emissions from internally feeding larvae to count infested wheat kernels in grain samples. Appl. Acoust. 50 (4), 297–308.
Wu, Z.H., Huang, N.E., 2009. Ensemble empirical mode decomposition: a noise-assisted data analysis method. Adv. Adapt. Data Anal. 1 (1), 1–41.
Wang, H.C., Chen, J., Dong, G.M., 2014. Feature extraction of rolling bearing's early weak fault based on EEMD and tunable Q-factor wavelet transform. Mech. Syst. Signal Process. 48 (1–2), 103–119.